

Acid-Doped Hydrogel Electrolytes for Electrocatalyst Interfaces

Adlai Katzenberg, Cesar Muñoz Davila, Brian Chen, Tana Siboonruang, and Miguel A. Modestino*

Cite This: *ACS Appl. Polym. Mater.* 2020, 2, 2046–2054

Read Online

ACCESS |



Metrics & More



Article Recommendations



Supporting Information

ABSTRACT: Polymer–electrolyte membranes (PEMs) are ubiquitous to state-of-the-art electrochemical devices (i.e., fuel cells and water electrolyzers). Stable PEMs have been historically limited to a small class of perfluorinated sulfonic acid ionomers (PFSA), which are expensive, difficult to synthesize, and have several key mass-transport limitations that restrict the achievable current densities in PEM devices. Specifically, structural changes in PFSA ionomers observed under low humidity and confined length scales (<100 nm thin films) limit proton conduction and mass-transport rates in the catalyst layer (CL) of PEM devices. We propose an alternative class of polymer electrolyte based on a low-cost polymer scaffold cross-linked and doped with an inorganic acidic charge carrier. As a model material system, we demonstrate a thermally cross-linked poly(acrylic acid)–poly(vinyl alcohol) network doped with sulfuric acid, with charge carrier concentration tuned via the dopant concentration. By implementing a chemically cross-linked scaffold and high dopant concentrations, we achieved a proton concentration of over 15 mmol g^{-1} , more than 10 times higher than available PFSA. The dopant concentration strongly impacted the polymer's water swelling ratio, higher than 70% in a highly doped material, and proton conductivity, as high as 350 mS cm^{-1} . Notably, the high proton conductivity was maintained even in confined thin films and across humidity levels relevant to PEM fuel cells (PEMFC) and electrolyzer operation. The doped hydrogel electrolyte was employed in a microelectrode vapor-fed water electrolyzer and achieved current densities up to several orders of magnitude higher than Nafion, the most widely implemented PFSA. The results demonstrate the potential for improved polymer electrolyte devices by utilizing low-cost materials tailored to specific device requirements.

KEYWORDS: polymer electrolyte, ionomer, hydrogel, thin film, confinement, water electrolysis

INTRODUCTION

The thrust to develop efficient solutions for energy conversion and storage has produced substantial improvements in polymer–electrolyte-based fuel cells (PEFC) and electrolyzers in the past decades.¹ These improvements have largely been driven by the remarkable transport properties of a class of perfluorinated sulfonic acids (PFSA) ion-conducting polymers, or PFSA ionomers, such as Nafion.^{2,3} These ionomers phase separate into a network of ion-conducting hydrophilic channels embedded in a perfluorinated matrix. This nanostructure imparts high proton conductivity but is sensitive to humidity and thin-film confinement effects, causing drastic disparity in PFSA properties depending on their surrounding environment and processing conditions.^{3–21} Specifically, structural changes in PFSA ionomers observed under low humidity and confined length scales (i.e., <100 nm thin films) limit proton conduction and water transport rates in the catalyst layer of PEM devices.^{7,10,22–26} Coupled with the complex morphology of catalyst layers,²⁷ in which ionomer coverage and water content vary stochastically, this makes it challenging to predict, model, and optimize ionomer performance during operation. As the limitations of Nafion have become clear, the research community has started to focus on

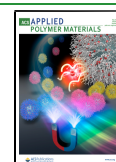
the development of alternative PFSA with transport properties more suitable for catalyst layers.^{23,25,28–30} One of the primary goals in ionomer development has been to increase conductivity, generally via increased concentration of acid groups. The tethered anionic groups are known to interact strongly with platinum, impacting local ionomer structure and electrode performance.^{14,31–36} Increased acid content can be reasonably expected to exacerbate these effects.

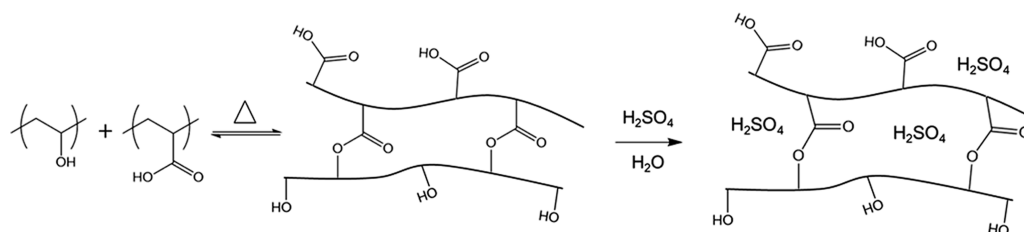
The PFSA-fluorinated structure imparts chemical stability, which is essential in oxidative environments but adds cost and complexity to the synthesis of ionomers. This oxidative stability is not required in all of the components of electrochemical devices; for example, PEFC anodes and PEM electrolyzer cathodes operate at low potentials ($\sim 0 \text{ V}$) and are not exposed to oxidizing species. These components could operate with nonfluorinated ionomers, enabling the

Received: February 28, 2020

Accepted: April 16, 2020

Published: April 16, 2020



Scheme 1. Fabrication of Sulfuric Acid-Doped PAA/PVA Networks^a

^aPAA and PVA are cross-linked by ester bonds and then swollen with H_2SO_4 . Hydrogel ionic strength can be controlled by H_2SO_4 concentration, enabling simple fabrication of polymer electrolytes with variable ionic strength.

incorporation of alternative inexpensive and tunable high-performing polymer electrolytes. The previous work on nonfluorinated ionomers has been tailored toward membranes, which do require oxidative stability and have thus not been widely implemented.³⁷

Polymer gel electrolytes have been developed for use in batteries and generally consist of a polymer scaffold, which provides mechanical integrity, swollen by a liquid electrolyte that imparts charge mobility.^{38,39} Such materials have gained traction for their low volatility^{40,41} and tendency to limit dendrite formation.^{42–44} Polymer gel electrolytes suffer a few key limitations in battery applications including lower conductivity than liquid electrolytes, low electrochemical stability, and typically require the use of organic solvents.^{45–50} These limitations are not present in fuel cell and electrolyzer catalyst layers where the mobility of H^+ ions is high, water can be used as a solvent, and oxidative stability is not required in some of the electrodes. Given the potential advantages of polymer gel electrolytes, we explored hydrocarbon-based hydrogel scaffolds doped with inorganic acids as a tunable material platform for fuel cell or electrolyzer catalyst layers. As a model material, we used cross-linked networks of poly(acrylic acid) (PAA) and poly(vinyl alcohol) (PVA) doped with aqueous sulfuric acid (H_2SO_4) solutions (Scheme 1). This material leverages the mechanical stability of a cross-linked hydrogel with the high ionic conductivity of aqueous electrolytes. Additionally, due to the homogeneous nature of this gel microstructure, thin-film confinement limitations are expected to be reduced in comparison to typical PFSA ionomers (Figure 1).

RESULTS AND DISCUSSION

Interactions of PAA/PVA and Dopant Sulfuric Acid.

Cross-link stability is a crucial consideration in polymer gel electrolytes to prevent dissolution of the ionomer in the catalyst layers. Doping thermally cross-linked PAA/PVA gels with sulfuric acid can result in the cleavage of ester cross-links via hydrolysis. Cross-link stability at room temperature was evaluated by attenuated total reflectance–Fourier transform infrared (ATR–FTIR) spectroscopy of doped hydrogels (Figure 2a). The C–O–C vibration from ester bonds has been previously attributed to an IR absorbance peak around 1150 cm^{-1} ,⁵¹ which is observed in cross-linked PAA/PVA (blue) and to a lesser extent in the non-cross-linked blend (green). This peak exhibited an initial decrease in intensity upon submerging the material in 1 M sulfuric acid, which may be due to absorbance attenuation by the incorporation of the electrolyte or ester hydrolysis. After this initial decay, the ester peak persisted over long treatment times of up to 66 h (Figure 2b), indicating that the hydrolysis is sufficiently slow at room

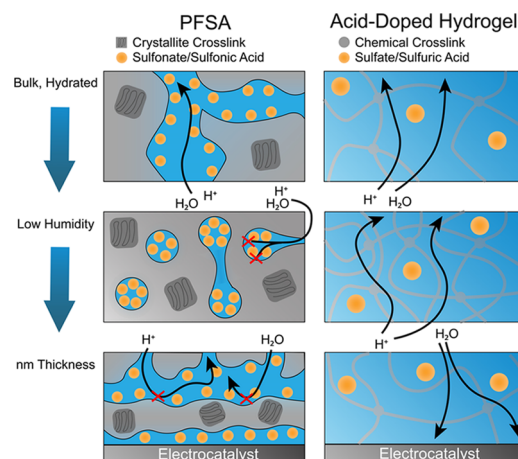


Figure 1. PFSA-transport properties (i.e., proton conductivity and water diffusivity) are highly sensitive to humidity and thin-film confinement because they are tied to a complex phase-separated nanostructure. This environmental sensitivity impacts the ionomer performance in catalyst layers in ways which are well documented but difficult to predict and control. The model polymer electrolyte studied in this work implements a PAA/PVA hydrogel doped with H_2SO_4 . This material displayed superior confinement and humidity tolerance via a homogeneous charge transport, which is not tied to the hydration-dependent nanostructure.

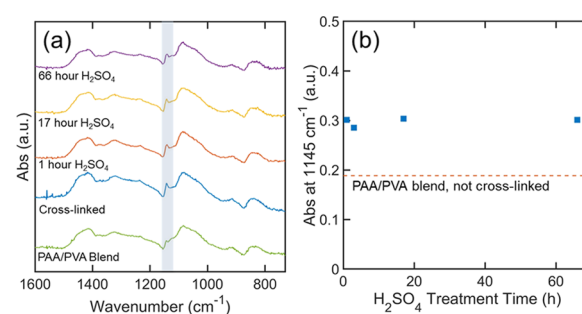


Figure 2. (a) ATR–FTIR spectra of bulk PAA/PVA hydrogels displayed an absorbance peak at 1145 cm^{-1} (highlighted in blue) attributed to the C–O–C vibration of the ester bond formed during thermal cross-linking. (b) This peak persisted upon treating the material with 1 M H_2SO_4 , indicating that acid-catalyzed hydrolysis of ester bonds proceeded slowly at room temperature.

temperature to ensure cross-link stability on the time scale of several days.

The ability to tune charge carrier (e.g., protons) concentration is critical in ionomer design, as ionic strength impacts the electrolyte water sorption and conductivity. In our material system, the proton concentration is determined by the

number of deprotonated acid moieties in the polymer scaffold and the concentration of dopant ions. Since the dopants used in this study (1, 0.1, and 0.01 M sulfuric acid) have pH well below the pK_a of PAA and PVA, most acidic polymer functional groups are expected to be protonated and the ionic strength of the doped hydrogel is dominated by acid uptake. Acid uptake of PAA/PVA thin films doped with a range of H_2SO_4 concentrations is presented in Figure 3 (blue

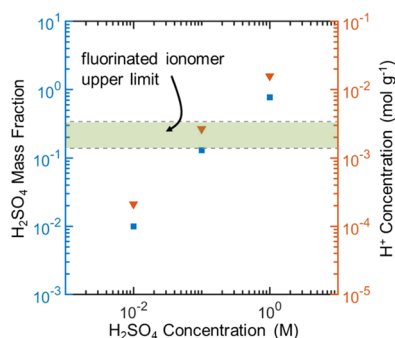


Figure 3. Quartz-crystal microbalance (QCM) measurements show that mass uptake (left axis) and estimated proton concentration (right) of acid-doped PAA/PVA hydrogel films scaled with H_2SO_4 concentration. Notably, higher proton concentration was measured for these materials than can be achieved in PFSA (the green region indicates a proposed upper limit for fluorinated ionomers²⁸) without compromising stability in aqueous environments. Measurements were averaged over at least 10 min, with less than 1% deviation.

squares). The mass of each film was measured after cross-linking and rinsing in water and then again after 1 h equilibrating in the respective H_2SO_4 solution. The fractional mass increase under dry N_2 flow (i.e., the mass uptake of sulfuric acid) was directly proportional to the concentration of sulfuric acid in the dopant solution. Notably, the fractional mass increase for 1 M H_2SO_4 was 3.4, indicating that more than 75% of the film's mass corresponded to sulfuric acid. From the fractional mass increase, proton concentration ($mol\ H^+ g^{-1}$ electrolyte) was estimated, assuming no contribution from the polymer, as double the number of moles of absorbed H_2SO_4 divided by the total weight of the doped (and dried) film. This is analogous to ion-exchange capacity (IEC) commonly referenced for PFSA ionomers and other ion-exchange resins with tethered anions. As shown in Figure 3 (orange triangles), proton concentration reached values $>15\ mmol\ g^{-1}$ at high H_2SO_4 concentration, a factor of 12 higher than available formulations of Nafion. In PFSA ionomers, IEC is limited by solubility/stability concerns. PFSA water solubility is promoted by sulfonic acid incorporation and restricted by crystallites in the poly(tetrafluoroethylene) (PTFE) matrix, which act as physical cross-links. At high PFSA fractions, crystallinity of the ionomer becomes compromised, resulting in loss of mechanical strength and representing an upper limit for IEC.¹⁹ A proposed upper limit for fluorinated ionomers including emerging side-chain chemistries²⁸ is indicated by the green region in Figure 3. In H_2SO_4 -doped PAA/PVA, the chemical cross-links are decoupled from ionic strength, enabling higher proton concentration without compromising stability.

Humidity and Thickness Dependence of Water Uptake and Ionic Conductivity. Water absorption in soft materials is driven by the difference in chemical potential of

water in the environment (i.e., the gas phase humidity) and in the material (i.e., affected by the ionic strength). This driving force is modulated by mechanical deformation energy required for expansion of the polymer network during swelling.²¹ Water swelling in doped hydrogels is important because the conductivity of the film is dictated by both (a) the concentration of mobile charge carriers and (b) the mobility of these charge carriers in the swollen hydrogel. Carrier concentration scales with the dopant concentration, and thus higher values of water uptake would decrease ionic conductivity. At the same time, water sorption reduces the volume fraction of the polymer in the material, increasing the volume fraction of the mobile phase within the gel and thus enhancing charge carrier mobility.^{52–54}

Humidity response of (a) conductivity and (b) swelling of acid-doped PAA/PVA gels is shown in Figure 4. Films (8–18

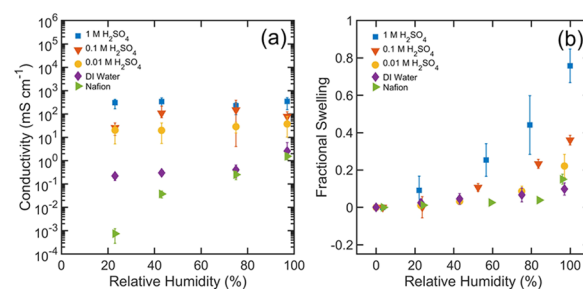


Figure 4. Conductivity and swelling fraction of sulfuric acid-doped PAA/PVA hydrogel thin films (18 nm) at room temperature as a function of relative humidity. (a) Acid-doped PAA/PVA exhibited conductivities as high as $350\ mS\ cm^{-1}$, with no clear humidity dependence. Nafion has been demonstrated to exhibit significant humidity dependence, which is exacerbated in thin films. (b) Swelling response of 8–18 nm doped PAA/PVA and Nafion (green triangles). Acid-doped gels exhibited a greater fractional swelling than Nafion at all humidities. Error bars represent the standard deviation of measurements of at least three samples.

nm) were studied to match the length scale of ionomer films in catalyst layers,²⁷ and all measurements were performed at room temperature. Nafion is presented for comparison, and the measured values are consistent with the prior literature on ionomer thin films.^{6,12,55} The conductivity of these materials exhibited no clear humidity dependence but was strongly correlated to dopant acid concentration. This is consistent with the competing effects of water sorption on concentration and mobility of charge carriers, which appeared to offset each other in this case. This is in stark contrast to Nafion, which exhibited substantial sensitivity of conductivity to the hydration state. At high humidity, the conductivity of Nafion was similar to that of PAA/PVA with low dopant concentrations (0.01 M), $\sim 2\ mS\ cm^{-1}$. Approaching 20% relative humidity (RH), Nafion's conductivity dropped to $\sim 10^{-4}\ mS\ cm^{-1}$, while the PAA/PVA gel conductivity was only mildly impacted. In the case of PFSA, the water content impacts the nanostructure, as ionic domains display poor connectivity at low hydration.^{16,56,57} These drastic changes in morphology and conductivity at low humidity are not observed in doped PAA/PVA. The highest-ionic-strength material, doped with 1 M H_2SO_4 , exhibited conductivity as high as $350\ mS\ cm^{-1}$, a factor of 220 higher than Nafion at comparable thickness and humidity.

Fractional swelling, measured by ellipsometry, scaled predictably with the dopant concentration and humidity,

which are the driving forces for water sorption. As expected, chemically cross-linked hydrogels with high ionic strength exhibited high swelling fractions. The observed swelling fractions, nearly 0.8 for the 1 M doped material at 97% relative humidity, are much higher than those seen in PFSA and help to explain the high ionic conductivity observed. Comparison is challenging for low acid concentration (deionized (DI) water and 0.01 M H_2SO_4) and low humidity (<40% RH) because the observed swelling fractions were within experimental error.

The impact of thickness confinement on conductivity of doped PAA/PVA films was studied for thicknesses ranging from 8 to 97 nm, encompassing the typical catalyst layer (CL) ionomer length scales. Hydrogel films maintained high proton conductivity across the length scale, while Nafion's conductivity decreased by several orders of magnitude (Figure 5).

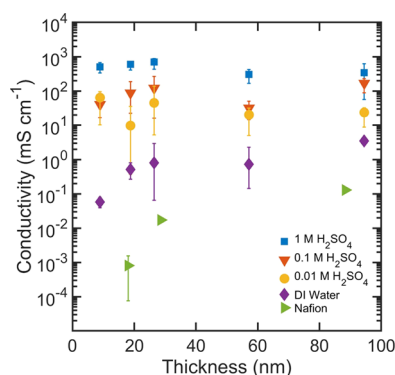


Figure 5. Conductivity of electrolyte-swollen PAA/PVA films at thicknesses ranging from 8 to 97 nm at 23% RH as determined by electrochemical impedance spectroscopy (EIS). Conductivity values did not change substantially as film thickness decreased but were sensitive to the acid dopant concentration. Nafion (green triangles) displayed a much stronger confinement-driven conductivity decrease. Error bars represent the standard deviation of measurements of at least three samples.

This observation is a direct result of confinement and interfacial interactions, which disrupt the nanophase separation of Nafion near the interface. In PFSA, charge transport occurs through ionic domains formed by phase separation; confinement disrupts the formation of these domains and hinders proton conduction in the material.⁶ A doped hydrogel, however, is homogeneously hydrated with a low polymer volume fraction, and thus charge transport is distributed throughout the material, consistent with the low sensitivity to thickness variations observed in Figure 5.

Evaluation of Electrochemical Performance. The transport properties of acid-doped PAA/PVA hydrogels and

their persistence across humidity and length scales suggest that they are well optimized toward implementation in electrochemical catalyst layers. Catalyst layer performance is sensitive to a myriad of processing parameters including (but not limited to) ink formulation, ionomer thickness and dispersion, and thermal history.^{36,58–61} These processing parameters will necessarily differ when fabricating PAA/PVA-based CLs and subsequent doping with H_2SO_4 , which complicates quantitative comparison of binder performance. To assess electrochemical performance in a well-controlled environment, which isolates the role of the binder, we employed two-dimensional (2-D) planar interdigitated microelectrodes (IDEs) in a water vapor-fed reactor.⁶² These IDEs have a similar geometry to the ones used to measure conductivity, but with wide electrode (100 μm) and small interelectrode spacing (10 μm) to enhance the surface area for electrochemical reactions and reduce resistance. Polymer films were spin-cast on the IDEs to produce films of uniform and controlled thickness. In this configuration, the anodic and cathodic microelectrodes are connected ionically via the ionomer thin film, while they remain electrically insulated from each other (Figure 6). Iridium electrodes were implemented to minimize the activation overpotential of the oxygen evolution reaction in the anode, which is significantly higher than the cathodic overpotential.⁶³ Given the low concentration of water in the electrolyzer (around 1 mM at standard temperature and pressure (STP) for saturated water vapor), limiting current density in this configuration is dictated by the flux of water through the ionomer film. While this model system is not consistent with the environment and engineering considerations of a PEM electrolyzer, it minimizes the challenges involved with implementing new materials in catalyst layers to enable a consistent exploration of the ionomer material space. Specifically, it enables a systematic study of electrochemical performance of the binder as a function of thickness, humidity, and other environmental parameters with the ability to distinguish between ohmic and mass-transport contributions.

Current density toward water splitting is dictated by two transport processes: proton conduction (which determines the ohmic overpotential) and water transport (which determines the flux of water from bulk to the anode surface). In the case of Nafion, the interplay of humidity, thickness/confinement, and nanostructure strongly impact these processes. At low humidity and under confinement (<100 nm), percolation of the hydrophilic domains is inhibited,^{15,18} resulting in substantially decreased proton conductivity, as demonstrated in this study and numerous others.^{11,17,55} This results in increased ohmic overpotential, which reduces the current density at a given applied voltage. Water transport proceeds through the same hydrophilic domains as proton transport;

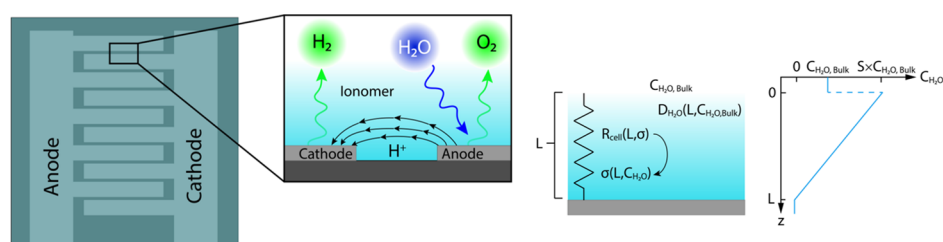


Figure 6. Schematic of the IDE microelectrode electrochemical test environment used to probe binder performance. Polymer thin films facilitate transport of reactants from bulk to the anode surface and of protons between the anode and cathode.

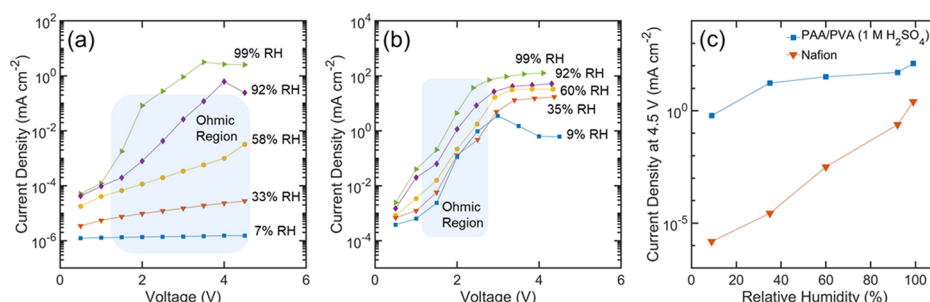


Figure 7. Polarization curves of (a) 102 nm Nafion and (b) 93 nm PAA/PVA doped with 1 M H₂SO₄ on iridium IDEs employed in water electrolysis. While the PAA/PVA binders displayed minimal sensitivity to humidity, Nafion's humidity sensitivity was very pronounced. (c) Current density at 4.5 V demonstrates the impact of humidity in limiting current density. Current densities were averaged over 2 min and all standard deviations were below 6% of the average value.

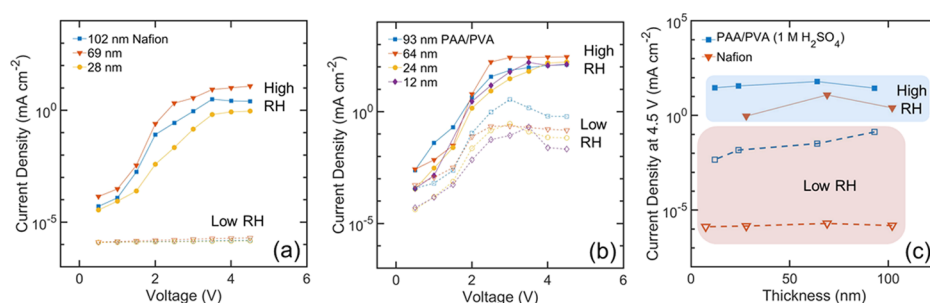


Figure 8. Polarization curves for (a) Nafion and (b) PAA/PVA doped with 1 M H₂SO₄ at thicknesses ranging from 100 to <10 nm (filled: >95% RH, empty: <10% RH). (c) Water-splitting current density at 4.5 V. Both ionomers showed strong performance sensitivity to relative humidity, although the difference was much more pronounced for Nafion. At low humidity, PAA/PVA demonstrated decreased current density at low thicknesses, while Nafion did not. This is likely due to excessive ohmic overpotential for ultrathin dehydrated Nafion. Current densities were averaged over 2 min and all standard deviations were below 4% of the average value.

thus, the loss of the nanostructure also coincides with a reduction in water diffusivity.⁷ These structural changes limit the flux of water through the binder, restricting the limiting current density. This effect is especially pronounced at low humidity, where the percolation of hydrophilic domains is compromised.

Polarization curves of acid-doped PAA/PVA and Nafion on iridium IDEs at a range of humidities are shown in Figure 7. Current density with 102 nm Nafion films (Figure 7a) displayed a strong dependence on relative humidity, while 93 nm PAA/PVA (1 M H₂SO₄) (Figure 7b) exhibited a much weaker dependence. The impact of hydration on Nafion's performance is clear in several features of the polarization curves. First, the slope in the ohmic-controlled region is clearly sensitive to hydration. This points to the correlation between hydration and proton conductivity, resulting in increased cell resistance at low humidity. In fact, the cell resistance ranged from 2.3 MΩ (low humidity) to 2 kΩ (high humidity). The onset voltage for water splitting appears to decrease with increasing humidity due to the large ohmic drop in poorly conducting ionomers. Neither of these effects was observed in the IDEs coated with PAA/PVA electrolytes. The ohmic-controlled regions displayed similar slope for all humidities given the weak effects of humidity in the conductivity of this material. The microelectrolyzers reach limiting current density at voltages above 3 V due to water transport. These limiting current densities (measured at 4.5 V) are shown in Figure 7c. For both PAA/PVA and Nafion, the limiting current density increased with humidity due to the change in water concentration in the gas phase. The humidity effects on limiting currents were more pronounced for Nafion, as

transport limitations are exacerbated by reduction in water diffusivity at low humidity. It is important to note that even at high humidity, where the transport limitations in Nafion are minimized, the device employing PAA/PVA still achieved over 10 times the current density in the device employing Nafion. This is consistent with the high conductivity, water content, and proton concentration of doped PAA/PVA films. At low humidity, this difference is much more pronounced, reaching an increase of over 5 orders of magnitude in limiting current density.

Ionomer thickness also has significant implications for electrochemical performance given the thickness-dependent transport properties of Nafion. In the case of water splitting on adjacent planar electrodes, the ionomer acts as the electrolyte and a transport resistance for water. Confinement effects coupled with geometric resistance scaling suggest that Nafion thin-film electrolytes should exhibit significant ohmic overpotential. As a mass-transport barrier, competing scaling effects are expected. Ion transport resistance scales inversely with film thickness, but water diffusivity in Nafion has been shown to decrease due to confinement^{7,64} while water sorption increases.^{7,31,65} In the case of PAA/PVA, due to the geometry of the electrolyzers, the electrolyte conductance and water permeance are inversely proportional to film thickness. By operating the μ IDE electrolyzer with ionomer films of varying thickness, we were able to assess the performance implications of these coupled processes.

Figure 8 shows the water-splitting performance for ionomer films ranging from <10 to ~100 nm in thickness. Blue markers indicate PAA/PVA (1 M H₂SO₄) and red markers indicate Nafion, with squares and triangles indicating high (99%) and

low (<10%) relative humidity, respectively. Polarization curves shown in Figure 8a,b demonstrate substantial performance differences between the two binders. At low humidity, current density in the Nafion electrolyzers was on the order of nA cm^{-2} for all thicknesses. This low current density is due to the limited water availability, device geometry, humidity-driven loss of conductivity, and confinement-driven loss of conductivity, which result in large overpotentials. PAA/PVA exhibited higher current densities at low humidity. Robust ionic conductivity across the humidity and length scale helped to mitigate ohmic losses, as cell resistance ranged from $10\ \Omega$ (thickest film, highest humidity) to $8.2\ \text{k}\Omega$ (thinnest film, lowest humidity), while robust water sorption across the humidity scale helped maintain reactant availability. In contrast, the cell resistance in Nafion films ranged from $2\ \text{k}\Omega$ to $10\ \text{M}\Omega$ across the same range of thicknesses and humidity.

At high humidity, Nafion films achieved much higher limiting current densities than at low humidity (Figure 8c). PAA/PVA also exhibited higher limiting current density, but the differences were less pronounced. This underscores the complexity of the relationship between the length scale, nanostructure, transport rates, and electrochemical performance in Nafion, which are greatly simplified in a structurally homogeneous hydrogel such as PAA/PVA.

A significant advantage of doped hydrogels is the ability to readily tune their ionic strength through the dopant concentration. Ionic strength strongly influences conductivity and water uptake, both of which affect the electrochemical performance of microelectrolyzers (Figure 9a). The slope in

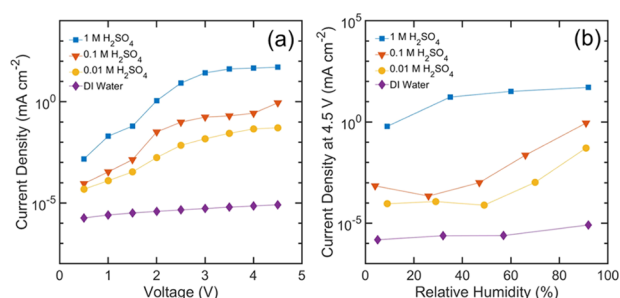


Figure 9. (a) Polarization curves for PAA/PVA thin films doped with different electrolyte concentrations show strong impact of ionomer proton concentration on electrochemical performance toward water splitting. At higher acid concentrations, these electrolyzers displayed improved ohmic performance and limiting current density. (b) Limiting current density was sensitive to the dopant concentration and humidity. Current densities were averaged over 2 min and all standard deviations were below 8% of the average value.

the ohmic-controlled region (i.e., below 1.5 V) clearly increased with increasing acid concentration, due to higher electrolyte conductivity. Cell resistance measurements are consistent with this observation, ranging from $340\ \text{k}\Omega$ for undoped films to $15\ \Omega$ in the $1\ \text{M H}_2\text{SO}_4$ doped film. Likewise, the limiting current density, attributed to water transport rates in the ionomer, increased from $8.5\ \mu\text{A cm}^{-2}$ to $27\ \text{mA cm}^{-2}$. The impact of water transport in device performance is evident, as there was a clear decrease in limiting current density at reduced humidity (Figure 9b) for all dopant concentrations.

CONCLUSIONS

This study explored the properties of PAA/PVA cross-linked networks doped with sulfuric acid as a polymer electrolyte designed for fuel cell or electrolysis catalyst layers. Electrolyte ionic strength was controlled by the concentration of the dopant acid and strongly influenced ionic conductivity and water sorption. Strong acid concentrations enabled higher proton concentration than has been achieved in PFSA, leading to conductivity as high as $350\ \text{mS cm}^{-1}$ in hydrogel thin films (<100 nm), which persisted under subambient humidity. A microelectrode-based test system was employed to evaluate ionomer performance under electrochemical operation across the same range of thickness and humidity, particularly relevant for electrochemical catalyst layers. Nafion electrolytes exhibited substantial reduction in current density at <10% RH (i.e., >6 orders of magnitude), while doped PAA/PVA maintained similar current density across thicknesses ranging from 7 to 100 nm and low sensitivity to humidity (i.e., exhibiting a reduction of <2 orders of magnitude from 99 to <10% RH). These results underscore the limitations of Nafion as a catalyst binder and provide a platform for facile formulation of improved ionomers based on polymer networks swollen with tunable aqueous electrolytes.

EXPERIMENTAL SECTION

Materials. All chemical reagents referenced below were purchased from Sigma-Aldrich (St. Louis, MO) unless otherwise noted.

Thin-Film Hydrogel Preparation. PAA/PVA hydrogels were prepared by spin casting a blend of PVA ($89\,000\text{--}98\,000\ \text{g mol}^{-1}$) and PAA ($250\,000\ \text{g mol}^{-1}$) in a 4:1 ratio, respectively, dissolved in water between 0.25 and 4 wt % on Si or quartz substrates at 4000 rpm for 1 min. Prior to spin casting, substrates were cleaned by sonicating in acetone followed by isopropyl alcohol (IPA), rinsed with DI water, and cleaned with O_2 plasma for 10 min. Film thickness was controlled by varying the concentration of the polymer in solution. These films were then cross-linked for 1 h at $130\ ^\circ\text{C}$ under vacuum to drive esterification of carboxylic acid and alcohol moieties by following the procedure outlined by Richter et al.⁶⁶ Cross-linked films were then submerged in sulfuric acid at a desired concentration ranging from 0 to 1 M for 1 h. Films were removed from the acid and dried by spin casting at 4000 rpm for 1 min to remove excess solution. Nafion films were prepared by spin casting on Si from 0.1 to 3 wt % solutions (prepared from Nafion D2021, Fuel Cell Store) in 70% IPA in water at 4000 rpm for 1 min and were annealed at $160\ ^\circ\text{C}$ for 1 h.

ATR-FTIR Analysis of Cross-link Stability. Bulk PAA/PVA hydrogels were prepared by drop-casting PAA/PVA at 13.5 wt % in water on glass cover slips and allowing the water to dry slowly at room temperature. An initial ATR-FTIR spectrum was captured of the dried blend. The dried films were then cross-linked at $130\ ^\circ\text{C}$ under vacuum. After cross-linking, the films were peeled off the glass slides and another spectrum was collected. The hydrogels were then submerged in 1 M sulfuric acid for variable times and then washed in a large deionized water bath for 1 h before drying at $50\ ^\circ\text{C}$ for 1 h before collecting the final spectrum. ATR-FTIR spectra were collected with a Thermo Scientific Nicolet 6700 FTIR in ATR mode. Per sample, 50 scans were collected and the absorbance was averaged. Background spectra (50 scans) were collected before each sample.

Acid Uptake Measurements. Acid uptake was measured by spin casting PAA/PVA films from 2 wt % in water on 10 MHz AT-cut quartz-crystal microbalance (QCM) crystals with evaporated gold electrodes (OpenQCM, nominal sensitivity $4.42 \times 10^{-9}\ \text{g Hz}^{-1}\ \text{cm}^{-2}$). Films were then cross-linked at $130\ ^\circ\text{C}$ under vacuum for 1 h. Immediately after cross-linking, films were submerged in DI water for 1 h, as negative mass change after doping was observed and attributed to leaching of the un-cross-linked polymer. The film area density was measured with an OpenQCM Fluidic Cell QCM under

dry N₂ flow at room temperature. The films were then submerged in the appropriate sulfuric acid concentration for 1 h, after which they were removed from solution and dried with N₂ flow. The post-doping area density was again measured under dry N₂ flow to determine the mass uptake of sulfuric acid. Proton concentration (c_{H^+}) was calculated as

$$c_{H^+} = 2 \frac{(\Delta m_{H_2SO_4})/MM_{H_2SO_4}}{m_0 + \Delta m_{H_2SO_4}} \quad (1)$$

where m_0 is the initial film area density, $\Delta m_{H_2SO_4}$ is the area density change after doping, and $MM_{H_2SO_4}$ is the molar mass of sulfuric acid.

Thin-film Swelling Measurements. Thickness and swelling measurements were taken with a Horiba UVISSEL Plus spectroscopic ellipsometer with relative humidity controlled by mixing humidified and dry gas streams. The humidified stream was generated by passing dry N₂ through two midjet impinger bubblers in series. The total flow rate (of the dry and humid stream) was maintained constant, and the humidity was controlled by the ratio of the two streams as controlled by two Sho-Rate series variable area flow meters (Brooks Instruments). Samples were housed in a sealed cell with quartz windows for in situ ellipsometry. Relative humidity immediately upstream of the sample cell was measured with an Adafruit DHT22 humidity sensor with $\pm 3\%$ accuracy.

Thin-film Conductivity Measurements. For conductivity measurements, platinum interdigitated electrodes (IDEs) were fabricated at the NYU Tandon Nanofab Cleanroom on 100 mm silicon wafer (UniversityWafer, 250 nm thermally grown oxide layer). Platinum (200 nm) and 20 nm titanium (for adhesion) were sputtered in a Kurt Lesker physical vapor deposition cluster tool. Planar interdigitated electrodes were patterned with AZ 5214 E photoresist (Microchemicals GmbH) and SÜSS Microtec MA 6 contact aligner followed by ion beam etching (Int'lVac Nanoquest II). Patterned electrodes were then diced into 1 cm² squares with a Disco DAD3320 dicing saw at the City University of New York Advanced Science Research Center. Each set of IDEs had 39 pairs of teeth with 3 mm overlap length, 5 μ m width, and 100 μ m spacing.

IDE ohmic contacts were embedded in airtight 20 mL scintillation vial lids to enable humidity-controlled conductivity measurements. During conductivity measurements, humidity was controlled by adding a reservoir of saturated aqueous salt to the vial. The following salts were used: potassium acetate (23% RH), potassium carbonate (43% RH), sodium chloride (75% RH), and potassium sulfate (97% RH).⁶⁷ Films were allowed to equilibrate at least 24 h prior to measurement. Film resistance was determined by electrochemical impedance spectroscopy (EIS) and used to calculate ionomer conductivity as

$$\kappa_f = \frac{1}{R_f} \frac{d}{l(N-1)t}$$

where κ_f is the film conductivity, R_f is the resistance, t is the film thickness, d is the spacing between IDE teeth, l is the length of the teeth, and N is the number of teeth.^{17,55} Spectra were collected from 100 Hz to 7 MHz with 50 points per decade and 2 measurements per frequency. Film resistance was extracted from the impedance spectrum by fitting a semicircle to the high-frequency circular feature, according to previous analysis of PFSA films on similar IDEs.^{6,9,12,17} All measurements were taken at room temperature.

For water-splitting measurements, iridium IDEs were patterned with 37 pairs of teeth of 3 mm length, 100 μ m width, and 10 μ m spacing by following the same procedure outlined above. After film casting, samples were loaded in a 3-D-printed reactor consisting of a base and cover sealed with a rubber gasket. Gold pogo pins were embedded in the cover to enable connection to a potentiostat (Biologic VSP-300). Relative humidity was controlled by flow of mixed streams of dry and water-saturated N₂ at controlled ratios set with GF40 series mass flow controllers (Brooks Instruments). Humidity directly upstream of the reactor was measured with a DHT22 humidity and temperature sensor with $\pm 3\%$ accuracy.

Temperature was measured simultaneously and varied between 21.9 and 23.0 °C. Once the humidity stabilized, the sample was allowed to equilibrate for 1 h. Before each measurement, EIS spectra were collected from 100 Hz to 7 MHz with 50 points per decade and 2 measurements per frequency to determine cell resistance. Polarization curves were then collected by varying the cell voltage from 0 to 4.5 V at 5 min intervals of 0.5 V. Current was averaged over the last 2 min.

It should be noted that stability, conductivity, and electrolyzer performance for these materials were measured at room temperature, which is appropriate for comparison among thin-film ionomers but outside the standard operating conditions of PEM fuel cells and electrolyzers. Given the reversible nature of ester bonds, long-term stability may suffer at elevated temperature and could be addressed by the implementation of more robust covalent cross-links.

■ ASSOCIATED CONTENT


Supporting Information

The Supporting Information is available free of charge at <https://pubs.acs.org/doi/10.1021/acsapm.0c00214>.


Geometry of IDEs used in conductivity and water splitting experiments (PDF)

■ AUTHOR INFORMATION

Corresponding Author

Miguel A. Modestino – Tandon School of Engineering, New York University, Brooklyn, New York 11201, United States;
 orcid.org/0000-0003-2100-7335; Email: modestino@nyu.edu

Authors

Adlai Katzenberg – Tandon School of Engineering, New York University, Brooklyn, New York 11201, United States;
 orcid.org/0000-0002-4793-5853

Cesar Muñoz Davila – Tandon School of Engineering, New York University, Brooklyn, New York 11201, United States

Brian Chen – Tandon School of Engineering, New York University, Brooklyn, New York 11201, United States

Tana Siboonruang – Tandon School of Engineering, New York University, Brooklyn, New York 11201, United States

Complete contact information is available at:

<https://pubs.acs.org/doi/10.1021/acsapm.0c00214>

Notes

The authors declare no competing financial interest.

■ ACKNOWLEDGMENTS

This work was performed in part at the Advanced Science Research Center NanoFabrication Facility of the Graduate Center at the City University of New York. The authors would like to acknowledge the financial support of NYU Tandon School of Engineering through M. A. M. startup fund. The authors thank Prof. Kalle Levon for use of the FTIR spectrometer and Prof. Rastislav Levicky for use of the ellipsometer.

■ REFERENCES

- (1) U.S. Department of Energy Office of Energy Efficiency and Renewable Energy. Hydrogen Storage. <https://www.energy.gov/eere/fuelcells/hydrogen-storage> (accessed May 6, 2019).
- (2) Weber, A. Z.; Newman, J. Modeling Transport in Polymer-Electrolyte Fuel Cells. *Chem. Rev.* **2004**, *104*, 4679–4726.
- (3) Mauritz, K. A.; Moore, R. B. State of Understanding of Nafion. *Chem. Rev.* **2004**, *104*, 4535–4585.

- (4) Modestino, M. A.; Kusoglu, A.; Hexemer, A.; Weber, A. Z.; Segalman, R. A. Controlling Nafion Structure and Properties via Wetting Interactions. *Macromolecules* **2012**, *45*, 4681–4688.
- (5) Kushner, D. I.; Hickner, M. A. Substrate-Dependent Physical Aging of Confined Nafion Thin Films. *ACS Macro Lett.* **2018**, *7*, 223–227.
- (6) Modestino, M. A.; Paul, D. K.; Dishari, S.; Petrina, S. A.; Allen, F. I.; Hickner, M. A.; Karan, K.; Segalman, R. A.; Weber, A. Z. Self-Assembly and Transport Limitations in Confined Nafion Films. *Macromolecules* **2013**, *46*, 867–873.
- (7) Eastman, S. A.; Kim, S.; Page, K. A.; Rowe, B. W.; Kang, S.; Soles, C. L.; Yager, K. G. Effect of Confinement on Structure, Water Solubility, and Water Transport in Nafion Thin Films. *Macromolecules* **2012**, *45*, 7920–7930.
- (8) Kreuer, K. D.; Portale, G. A Critical Revision of the Nano-Morphology of Proton Conducting Ionomers and Polyelectrolytes for Fuel Cell Applications. *Adv. Funct. Mater.* **2013**, *23*, 5390–5397.
- (9) Paul, D.; Fraser, A.; Pearce, J.; Karan, K. Understanding the Ionomer Structure and the Proton Conduction Mechanism in PEFC Catalyst Layer: Adsorbed Nafion on Model Substrate. *ECS Trans.* **2011**, *41*, 1393–1406.
- (10) Weber, A. Z.; Kusoglu, A. Unexplained Transport Resistances for Low-Loaded Fuel-Cell Catalyst Layers. *J. Mater. Chem. A* **2014**, *2*, 17207–17211.
- (11) Nagao, Y. Highly Oriented Sulfonic Acid Groups in a Nafion Thin Film on Si Substrate. *J. Phys. Chem. C* **2013**, *117*, 3294–3297.
- (12) Paul, D. K.; Fraser, A.; Karan, K. Towards the Understanding of Proton Conduction Mechanism in PEMFC Catalyst Layer: Conductivity of Adsorbed Nafion Films. *Electrochem. Commun.* **2011**, *13*, 774–777.
- (13) Moukheiber, E.; De Moor, G.; Flandin, L.; Bas, C. Investigation of Ionomer Structure through Its Dependence on Ion Exchange Capacity (IEC). *J. Memb. Sci.* **2012**, *389*, 294–304.
- (14) Novitski, D.; Holdcroft, S. Determination of O₂ Mass Transport at the Pt | PFSA Ionomer Interface under Reduced Relative Humidity. *ACS Appl. Mater. Interfaces* **2015**, *7*, 27314–27323.
- (15) Allen, F. I.; Comolli, L. R.; Kusoglu, A.; Modestino, M. A.; Minor, A. M.; Weber, A. Z. Morphology of Hydrated As-Cast Nafion Revealed through Cryo Electron Tomography. *ACS Macro Lett.* **2015**, *4*, 1–5.
- (16) Hsu, W. Y.; Gierke, T. D. Ion Transport and Clustering in Nafion Perfluorinated Membranes. *J. Memb. Sci.* **1983**, *13*, 307–326.
- (17) Paul, D. K.; Karan, K.; Docoslis, A.; Giorgi, J. B.; Pearce, J. Characteristics of Self-Assembled Ultrathin Nafion Films. *Macromolecules* **2013**, *46*, 3461–3475.
- (18) Kusoglu, A.; Dursch, T. J.; Weber, A. Z. Nanostructure/Swelling Relationships of Bulk and Thin-Film PFSA Ionomers. *Adv. Funct. Mater.* **2016**, *26*, 4961–4975.
- (19) Kusoglu, A.; Weber, A. Z. New Insights into Perfluorinated Sulfonic-Acid Ionomers. *Chem. Rev.* **2017**, *117*, 987–1104.
- (20) Tesfaye, M.; Kushner, D. I.; McCloskey, B. D.; Weber, A. Z.; Kusoglu, A. Thermal Transitions in Perfluorosulfonated Ionomer Thin-Films. *ACS Macro Lett.* **2018**, *7*, 1237–1242.
- (21) Kusoglu, A.; Savagatrup, S.; Clark, K. T.; Weber, A. Z. Role of Mechanical Factors in Controlling the Structure-Function Relationship of PFSA Ionomers. *Macromolecules* **2012**, *45*, 7467–7476.
- (22) Spangler, F. B.; Phillips, A.; Schuler, T.; Tucker, M. C.; Weber, A. Z. Investigating Fuel-Cell Transport Limitations Using Hydrogen Limiting Current. *Int. J. Hydrogen Energy* **2017**, *42*, 13960–13969.
- (23) Holdcroft, S. Fuel Cell Catalyst Layers: A Polymer Science Perspective. *Chem. Mater.* **2014**, *26*, 381–393.
- (24) Jiang, R.; Mittelsteadt, C. K.; Gittleman, C. S. Through-Plane Proton Transport Resistance of Membrane and Ohmic Resistance Distribution in Fuel Cells. *J. Electrochem. Soc.* **2009**, *156*, 1440–1446.
- (25) Kongkanand, A.; Mathias, M. F. The Priority and Challenge of High-Power Performance of Low-Platinum Proton-Exchange Membrane Fuel Cells. *J. Phys. Chem. Lett.* **2016**, *7*, 1127–1137.
- (26) Kongkanand, A. Interfacial Water Transport Measurements in Nafion Thin Films Using a Quartz-Crystal Microbalance. *J. Phys. Chem. C* **2011**, *115*, 11318–11325.
- (27) Cetinbas, F. C.; Ahluwalia, R. K.; Kariuki, N.; De Andrade, V.; Fongalland, D.; Smith, L.; Sharman, J.; Ferreira, P.; Rasouli, S.; Myers, D. J. Hybrid Approach Combining Multiple Characterization Techniques and Simulations for Microstructural Analysis of Proton Exchange Membrane Fuel Cell Electrodes. *J. Power Sources* **2017**, *344*, 62–73.
- (28) Yandrasits, M. A.; Lindell, M. J.; Hamrock, S. J. New Directions in Perfluoroalkyl Sulfonic Acid-Based Proton-Exchange Membranes. *Curr. Opin. Electrochem.* **2019**, *18*, 90–98.
- (29) Katzenberg, A.; Chowdhury, A.; Fang, M.; Weber, A. Z.; Okamoto, Y.; Kusoglu, A.; Modestino, M. A. Highly Permeable Perfluorinated Sulfonic Acid Ionomers for Improved Electrochemical Devices: Insights into Structure–Property Relationships. *J. Am. Chem. Soc.* **2020**, *142*, 3742–3752.
- (30) Rolfi, A.; Oldani, C.; Merlo, L.; Facchi, D.; Ruffo, R. New Perfluorinated Ionomer with Improved Oxygen Permeability for Application in Cathode Polymeric Electrolyte Membrane Fuel Cell. *J. Power Sources* **2018**, *396*, 95–101.
- (31) Kusoglu, A.; Kushner, D.; Paul, D. K.; Karan, K.; Hickner, M. A.; Weber, A. Z. Impact of Substrate and Processing on Confinement of Nafion Thin Films. *Adv. Funct. Mater.* **2014**, *24*, 4763–4774.
- (32) Tesfaye, M.; Kushner, D. I.; Kusoglu, A. Interplay between Swelling Kinetics and Nanostructure in Perfluorosulfonic Acid Thin-Films: Role of Hygrothermal Aging. *ACS Appl. Polym. Mater.* **2019**, *1*, 631–635.
- (33) Zhang, C.; Davies, M.; Karan, K. Probing Interfacial Interactions of Nafion Ionomer: Thermal Expansion of Nafion Thin Films on Substrates of Different Hydrophilicity/Hydrophobicity. *J. Polym. Sci., Part B: Polym. Phys.* **2019**, *57*, 343–352.
- (34) Kudo, K.; Jinnouchi, R.; Morimoto, Y. Humidity and Temperature Dependences of Oxygen Transport Resistance of Nafion Thin Film on Platinum Electrode. *Electrochim. Acta* **2016**, *209*, 682–690.
- (35) Schuler, T.; Chowdhury, A.; Freiberg, A. T.; Sneed, B.; Spangler, F. B.; Tucker, M. C.; More, K. L.; Radke, C. J.; Weber, A. Z. Fuel-Cell Catalyst-Layer Resistance via Hydrogen Limiting-Current Measurements. *J. Electrochem. Soc.* **2019**, *166*, F3020–F3031.
- (36) Van Cleve, T.; Khandavalli, S.; Chowdhury, A.; Medina, S.; Pylypenko, S.; Wang, M.; More, K. L.; Kariuki, N.; Myers, D. J.; Weber, A. Z.; Mauger, S. A.; Ulshu, M.; Neyerlin, K. C. Dictating Pt-Based Electrocatalyst Performance in Polymer Electrolyte Fuel Cells, from Formulation to Application. *ACS Appl. Mater. Interfaces* **2019**, *11*, 46953–46964.
- (37) Hickner, M. A.; Ghassemi, H.; Kim, Y. S.; Einsla, B. R.; McGrath, J. E. Alternative Polymer Systems for Proton Exchange Membranes (PEMs). *Chem. Rev.* **2004**, *104*, 4587–4611.
- (38) Cheng, X.; Pan, J.; Zhao, Y.; Liao, M.; Peng, H. Gel Polymer Electrolytes for Electrochemical Energy Storage. *Adv. Energy Mater.* **2018**, *8*, No. 1702184.
- (39) Liang, S.; Yan, W.; Wu, X.; Zhang, Y.; Zhu, Y.; Wang, H.; Wu, Y. Gel Polymer Electrolytes for Lithium Ion Batteries: Fabrication, Characterization and Performance. *Solid State Ionics* **2018**, *318*, 2–18.
- (40) Zhou, D.; Liu, R.; Zhang, J.; Qi, X.; He, Y. B.; Li, B.; Yang, Q. H.; Hu, Y. S.; Kang, F. In Situ Synthesis of Hierarchical Poly(Ionic Liquid)-Based Solid Electrolytes for High-Safety Lithium-Ion and Sodium-Ion Batteries. *Nano Energy* **2017**, *33*, 45–54.
- (41) Armand, M. The History of Polymer Electrolytes. *Solid State Ionics* **1994**, *69*, 309–319.
- (42) Qin, B.; Liu, Z.; Ding, G.; Duan, Y.; Zhang, C.; Cui, G. A Single-Ion Gel Polymer Electrolyte System for Improving Cycle Performance of LiMn₂O₄ Battery at Elevated Temperatures. *Electrochim. Acta* **2014**, *141*, 167–172.
- (43) Liu, S.; Wang, H.; Imanishi, N.; Zhang, T.; Hirano, A.; Takeda, Y.; Yamamoto, O.; Yang, J. Effect of Co-Doping Nano-Silica Filler and N-Methyl-N-Propylpiperidinium Bis(Trifluoromethanesulfonyl)Imide into Polymer Electrolyte on Li Dendrite Formation in Li/Pol-

(Ethylene Oxide)-Li(CF₃SO₂)₂N/Li. *J. Power Sources* **2011**, *196*, 7681–7686.

(44) Lu, Q.; He, Y. B.; Yu, Q.; Li, B.; Kaneti, Y. V.; Yao, Y.; Kang, F.; Yang, Q. H. Dendrite-Free, High-Rate, Long-Life Lithium Metal Batteries with a 3D Cross-Linked Network Polymer Electrolyte. *Adv. Mater.* **2017**, *29*, No. 1604460.

(45) Liu, F.; Hashim, N. A.; Liu, Y.; Abed, M. R. M.; Li, K. Progress in the Production and Modification of PVDF Membranes. *J. Memb. Sci.* **2011**, *375*, 1–27.

(46) Thayumanasundaram, S.; Rangasamy, V. S.; Seo, J. W.; Locquet, J. P. Lithium Polymer Electrolytes Based on Sulfonated Poly(Ether Ether Ketone) for Lithium Polymer Batteries. *Eur. J. Inorg. Chem.* **2015**, *2015*, 5395–5404.

(47) Ashby, D. S.; DeBlock, R. H.; Lai, C. H.; Choi, C. S.; Dunn, B. S. Patternable, Solution-Processed Ionogels for Thin-Film Lithium-Ion Electrolytes. *Joule* **2017**, *1*, 344–358.

(48) Fergus, J. W. Ceramic and Polymeric Solid Electrolytes for Lithium-Ion Batteries. *J. Power Sources* **2010**, *195*, 4554–4569.

(49) Li, W.; Xing, Y.; Wu, Y.; Wang, J.; Chen, L.; Yang, G.; Tang, B. Study the Effect of Ion-Complex on the Properties of Composite Gel Polymer Electrolyte Based on Electrospun PVdF Nanofibrous Membrane. *Electrochim. Acta* **2015**, *151*, 289–296.

(50) Xiao, S. Y.; Yang, Y. Q.; Li, M. X.; Wang, F. X.; Chang, Z.; Wu, Y. P.; Liu, X. A Composite Membrane Based on a Biocompatible Cellulose as a Host of Gel Polymer Electrolyte for Lithium Ion Batteries. *J. Power Sources* **2014**, *270*, 53–58.

(51) Arndt, K.-F.; Richter, A.; Ludwig, S.; Zimmermann, J.; Kressler, J.; Kuckling, D.; Adler, H.-J. Poly(Vinyl Alcohol)/Poly(Acrylic Acid) Hydrogels: FT-IR Spectroscopic Characterization of Crosslinking Reaction and Work at Transition Point. *Acta Polym.* **1999**, *50*, 383–390.

(52) Amsden, B. Solute Diffusion within Hydrogels. Mechanisms and Models. *Macromolecules* **1998**, *31*, 8382–8395.

(53) Wu, Y.; Joseph, S.; Aluru, N. R. Effect of Cross-Linking on the Diffusion of Water, Ions, and Small Molecules in Hydrogels. *J. Phys. Chem. B* **2009**, *113*, 3512–3520.

(54) Luo, X.; Rojas-carbonell, S.; Yan, Y.; Kusoglu, A. Structure-Transport Relationships of Poly (Aryl Piperidinium) Anion-Exchange Membranes: Effect of Anions and Hydration. *J. Memb. Sci.* **2019**, *598*, No. 117680.

(55) Paul, D. K.; McCreery, R.; Karan, K. Proton Transport Property in Supported Nafion Nanothin Films by Electrochemical Impedance Spectroscopy. *J. Electrochem. Soc.* **2014**, *161*, F1395–F1402.

(56) Gierke, T. D.; Munn, G. E.; Wilson, F. C. The Morphology in Nafion Perfluorinated Membrane Products, as Determined by Wide- and Small-Angle x-Ray Studies. *J. Polym. Sci., Polym. Phys. Ed.* **1981**, *19*, 1687–1704.

(57) Kusoglu, A.; Modestino, M. A.; Hexemer, A.; Segalman, R. A.; Weber, A. Z. Subsecond Morphological Changes in Nafion during Water Uptake Detected by Small-Angle X-Ray Scattering. *ACS Macro Lett.* **2012**, *1*, 33–36.

(58) Balu, R.; Choudhury, N. R.; Mata, J. P.; De Campo, L.; Rehm, C.; Hill, A. J.; Dutta, N. K. Evolution of the Interfacial Structure of a Catalyst Ink with the Quality of the Dispersing Solvent: A Contrast Variation Small-Angle and Ultrasmall-Angle Neutron Scattering Investigation. *ACS Appl. Mater. Interfaces* **2019**, *11*, 9934–9946.

(59) Xu, W.; Scott, K. The Effects of Ionomer Content on PEM Water Electrolyser Membrane Electrode Assembly Performance. *Int. J. Hydrogen Energy* **2010**, *35*, 12029–12037.

(60) “Molly” Jhong, H.-R.; Brushett, F. R.; Kenis, P. J. A. The Effects of Catalyst Layer Deposition Methodology on Electrode Performance. *Adv. Energy Mater.* **2013**, *3*, 589–599.

(61) Doo, G.; Lee, J. H.; Yuk, S.; Choi, S.; Lee, D. H.; Lee, D. W.; Kim, H. G.; Kwon, S. H.; Lee, S. G.; Kim, H. T. Tuning the Ionomer Distribution in the Fuel Cell Catalyst Layer with Scaling the Ionomer Aggregate Size in Dispersion. *ACS Appl. Mater. Interfaces* **2018**, *10*, 17835–17841.

(62) Modestino, M. A.; Dumortier, M.; Hosseini Hashemi, S. M.; Haussener, S.; Moser, C.; Psaltis, D. Vapor-Fed Microfluidic Hydrogen Generator. *Lab Chip* **2015**, *15*, 2287–2296.

(63) McCrory, C. C. L.; Jung, S.; Ferrer, I. M.; Chatman, S. M.; Peters, J. C.; Jaramillo, T. F. Benchmarking Hydrogen Evolving Reaction and Oxygen Evolving Reaction Electrocatalysts for Solar Water Splitting Devices. *J. Am. Chem. Soc.* **2015**, *137*, 4347–4357.

(64) Krttil, P.; Trojáněk, A.; Samec, Z. Kinetics of Water Sorption in Nafionthin Films - Quartz Crystal Microbalance Study. *J. Phys. Chem. B* **2001**, *105*, 7979–7983.

(65) Dishari, S. K.; Hickner, M. A. Antiplasticization and Water Uptake of Nafion Thin Films. *ACS Macro Lett.* **2012**, *1*, 291–295.

(66) Richter, A.; Bund, A.; Keller, M.; Arndt, K. F. Characterization of a Microgravimetric Sensor Based on PH Sensitive Hydrogels. *Sens. Actuators, B* **2004**, *99*, 579–585.

(67) Greenspan, L. Humidity Fixed Points of Binary Saturated Aqueous Solutions. *J. Res. Natl. Bur. Stand., Sect. A* **1977**, *81A*, 89.